Synaptic Vesicles Studied by SAXS: Derivation and Validation of a Model Form Factor

2010 J. Phys.: Conf. Ser. 247 012015

(http://iopscience.iop.org/1742-6596/247/1/012015)

Journal of Physics: Conference Series **247** (2010) 012015 doi:10.1088/1742-6596/247/1/012015

Synaptic Vesicles Studied by SAXS: Derivation and Validation of a Model Form Factor

S Castorph[1], L Arleth[2], M Sztucki[3], U Vainio[4], S K Ghosh[1], M Holt[5], R Jahn[5] and T Salditt[1]

[1] Institut für Röntgenphysik, Georg-August-Universität Göttingen, Göttingen, D
[2] Biophysics, Faculty of Life Sciences, University of Copenhagen, Frederiksberg, DK
[3] European Synchrotron Radiation Facility, Grenoble, F
[4] Hamburger Synchrotronstrahlungslabor at Deutsches Elektronen-Synchrotron, Hamburg, D
[5] Max Planck Institut für Biophysikalische Chemie, Department of Neurobiology, Göttingen, D

E-mail: scastor@gwdg.de, tsaldit@gwdg.de

Abstract. We discuss different spherically symmetric and anisotropic form factor models and test them against high resolution synchrotron based small-angle x-ray scattering (SAXS) data from synaptic vesicles (SVs), isolated from rat brain. Anisotropy of the model form factors is found to be a key ingredient for the description of the native synaptic vesicle structure. We describe changes in structural parameters due to protease digestion of SVs, and present SAXS data of SVs recorded under different pH conditions.

1. Introduction

The release of neurotransmitters from neurons, in response to stimulation, forms the basis of biochemical communication in the nervous system. Neurotransmitters are stored in small membranous organelles, synaptic vesicles (SVs), within the presynaptic terminal. These vesicles undergo an elaborate cycle of fusion with the plasma membrane (releasing neurotransmitter), followed by retrieval and reformation and transport back to the plasma membrane for further rounds of fusion [1].

In recent years there has been enormous progress in our knowledge of the molecular composition and structure of SVs [2]. Recently, we have determined the average radial density profile $\rho(r)$, as well as the polydispersity function $p(R)$, on an absolute scale from small angle x-ray scattering (SAXS), with no free prefactors [3]. The density profile of the vesicle with an inner and outer protein layer has confirmed a previous modeling study of SVs based on biochemical studies of protein inventory and stochiometry as well as the crystal structures of the constituent proteins [2]. In addition, the best model fits to the SAXS curves required the presence of laterally anisotropic structures on the vesicle surface, indicative of large protein clusters.

In this work we present the full derivation of the form factors used and give a more detailed account of the comparison between different models as well as a more comprehensive overview of different SV data sets. In particular, we present different spherically symmetric form factors, which are then tested and falsified. In particular both radially symmetric and asymmetric density profiles consisting of three or five coupled Gaussians fail to describe the structure of

SVs. Contrarily, an anisotropic form factor representing a symmetric bilayer profile, consisting of three Gaussians, with Gaussian chains attached to the outside and inside describes the SV structure well. A form factor where the attached Gaussian chains are replaced by hard spheres shows qualitatively the same result. Further, we investigate the structural changes associated with protease digestion of protein residues on the surface of SVs, and compare scattering patterns from SVs recorded under different pH conditions.

2. Materials and Methods

2.1. Purification of Synaptic Vesicles

Synaptic vesicles from rat brain were purified following a purification protocol by Jahn et al., [2]. Samples were kept on water/ice mixtures until investigation by electron microscopy (EM). Samples for the SAXS measurements were snap frozen for transportation to the synchrotron. All samples retained the capacity to acidify, which is an important indication that the SV membranes are functionally intact [4]. The resulting SV stock solutions had a protein concentration in the range of $5.47 - 6.45$ μg/μl.

For the protease digested SVs, one sample was split in two following the usual purification. To one sample 0.1 μg Trypsin per μg protein was added and incubated at 37 °C for 60 minutes. The other sample was incubated the same time on ice as a control. Both samples were centrifuged at 3×10^5 g (average) for two hours. The pellets were then re-suspended in aqueous buffer of 100 mM KCl, 25 mM HEPES and 1 mM DTT at pH 7.40. Both the centrifugation and re-suspension followed similar steps from the usual purification protocol.

2.2. Preparation of DOPS Vesicles

Small unilamellar lipid vesicles were prepared by dissolving 1,2-Dioleoyl-sn-Glycero-3-Phosphatidilserine (DOPS) supplied by Avanti Polar Lipids (Alabaster, AL) at a concentration $c = 20$ mg/ml in ultrapure water (Milli-Q), and sonication to clarity (Sonoplus, Germany).

2.3. Small-Angle X-Ray Scattering

SAXS experiments were performed at the high brilliance undulator beamline ID-2 of the European Synchrotron Radiation Facility (ESRF) in Grenoble, France, and beamline B1 at the Doris III storage ring of HASYLAB at Deutsches Elektronen-Synchrotron, Hamburg, Germany. Both beamlines were operated under the beamline's standard conditions at 12.4 keV [5] and 9.0 keV [6] photon energy, respectively. The SV samples were at total protein concentrations of 2.74 μg/μl in aqueous buffer of 100 mM KCl, 25 mM HEPES and 1 mM DTT at pH 7.40. The samples were kept in a glass flow through capillary, or wax sealed glass capillary, with a diameter of 1.5 mm and a wall thickness of 0.01 mm.

At beamline ID-2, the diffraction patterns were recorded with a FReLoN CCD detector positioned 0.85 and 5 m behind the sample in an evacuated detector tube. Data were collected over a q-range from 0.016 to 5.5 nm^{-1}. Typical exposure times were 0.1 seconds. The 2D isotropic (powder average) diffraction pattern was corrected for the CCD dark current, offset of the analogue to digital converter, spacial distortion, detector sensitivity (flat-field), and was calibrated to the absolute scale (water reference) employing the procedure described in [5]. Data recorded at the two different detector distances were combined to give a corrected scattering curve $I(q)$ covering more than two orders of magnitude in q. Radiation damage was ruled out by comparison of scattering patterns recorded with different exposure times from 0.01 to 10 seconds. For the standard accumulation time, the absorbed dose during exposure was about 6.5×10^3 Gy. Dilution series revealed no measurable inter-particle correlations or aggregation for samples of a total protein concentration between 6.45 μg/μl and 1.29 μg/μl.

At beamline B1, the diffraction patterns were recorded with a multiwire proportional chamber gas detector (Gabriel), or a Pilatus 300k silicon single photon counting pixel array detector

positioned 935 and 3635 mm behind the sample. Data were collected over a q-range from 0.08 to 2.9 nm^{-1}. Typical exposure times were 30 minutes. The 2D isotropic (powder average) diffraction pattern was corrected for the dark current, fluctuations in primary intensity, spacial distortion, detector sensitivity / flat-field (only for Gabriel detector), and was calibrated to the absolute scale (glassy carbon reference) employing a similar procedure as described in [5]. Data recorded at the two different detector distances were combined to give a corrected scattering curve $I(q)$. Detector resolution effects could be ignored at both the ID-2, ESRF, and the B1, HASYLAB, measurements.

2.4. Cryo Electron Microscopy

To determine the relative size polydispersity $p(R)$ of the SV population independently from SAXS, cryo electron microscopy (cryo-EM) measurements were performed on vitrified SV solutions. In total, 559 SV were analyzed and R was determined from the diameter of the SV, measured from bilayer surface to bilayer surface. Independently, $p(R)$ was also confirmed by dynamic light scattering (data not shown).

2.5. Scattering Form Factor Models

The scattering cross section for a dilute, polydisperse system of particles of radius R with the number size distribution $p(R)$, the volumes $V(R)$, and the scattering form factor $P(q, R)$ is given by [7]

$$\frac{d\sigma(q)}{d\Omega} = \Delta\rho^2 \int_0^\infty p(R)V(R)^2 P(q,R)\, dR \ . \tag{1}$$

$V(R)$ is the dry volume of the particle defined as the total volume V_{tot} minus the volume of the solvent core V_{core}. In the SV models, a bimodal size distribution function $p(R)$ was employed as shown in Fig.2 (B). The branch of $p(R)$ around approximately $R = 20$ nm has been determined by cryo-EM (smoothed) [3]. The diameter of the SV was measured from bilayer surface to bilayer surface. The branch of $p(R)$ around approximately $R = 200$ nm was calculated as a freely varied Gaussian contribution with mean μ and standard deviation σ to account for the trace number of larger membranous particles in the sample. In the DOPS vesicle models, $p(R)$ was a freely varied Gaussian only. $\Delta\rho = M/V$ denotes the difference between the scattering length density of the solvent and the average scattering length density of the decorated bilayer. M will be used below as the total excess scattering length of a particle.

The form factor models derived in this work are built from a central bilayer profile [8, 9, 10] with added contributions on the inside (lumen) and outside of the SV model, accounting for the numerous proteins associated with the SV membrane. The spherically symmetric electron density profile of the bilayer is modeled by three concentric Gaussians [11], representing the head groups of the two lipid leaflets and the hydrophobic core. Note that protein residues associated with the head groups and trans-membrane protein segments are included in this contribution. The larger proteins, or protein clusters, of the inner and outer protein shells, which can be clearly seen in cryo-EM images [3] are (1) not explicitly integrated into the model (also an asymmetric bilayer profiles has been tested), or modeled by coronas of (2) concentric Gaussians, (3) hard spheres, (4) Gaussian chains [12] attached to the inner and outer sides of the bilayer, respectively [13, 14, 15, 16, 3]. The contribution of the hard spheres, or Gaussian chains, coronas explicitly introduces an in-plane structure to the models, breaking the spherical symmetry. The individual hard spheres or Gaussian chains are assumed to be perfectly uncorrelated, forming an ideal gas on the sphere. The extension of the additional concentric Gaussians, the hard spheres and the Gaussian chains in the radial direction might be interpreted as the thickness of the protein layers, whereas the lateral extension (parallel to the membrane tangent plane) of the hard spheres or Gaussian chains may reflect the in-plane size of individual proteins, protein clusters

and/or distinct lipid micro domains in a coarse grained sense. For the calculation of polydisperse populations, the local structure of the concentric bilayer profile and, depending on the model, the additional terms describing the protein coronas were kept constant for all population members. Least-squares fitting was performed using the "lsqnonlin" routine of MATLAB Optimization Toolbox (Version 7.5.0.342 (R2007b), The MathWorks Inc.), dedicated to solve non-linear least-squares problems. The quality of a model fit $f(x)$ with p free model parameters to N data points of experimentally estimated photon counts y_i with empirical variances σ_i^2 was assessed by the value of the *reduced* χ^2 given by

$$reduced\ \chi^2 = \frac{\sum_{i=1}^{N} \frac{(y_i - f(x_i))^2}{\sigma_i^2}}{N - p - 1} \ . \tag{2}$$

The variances σ_i^2 were calculated by propagating the counting errors from the photon counts of the individual detector pixels through the data reduction and correction process. Cross-correlations between pixels were neglected.

In addition to the parameters of the different models given in Tabs. 1, 2, and 3 three parameters reflecting the freely varied Gaussian component of $p(R)$, accounting for larger membranous particles in the SV samples, and a small constant background, were subject to optimization during the fitting procedure of the form factor models to $I(q)$. The part of $p(R)$ representing the size distribution of the SVs as obtained by cryo-EM [2, 3] was kept constant for all fits. For both branches of $p(R)$, the same form factor was used. In particular the bilayer profile parameters, the parameters of the additional concentric Gaussians, or the density of hard spheres or Gaussian chains per surface area ($N_c^{in}/(4\pi(R-D-R_g^{in})^2)$ and $N_c^{out}/(4\pi(R+R_g^{out})^2)$) were kept constant. The effective number of free parameters of the different models are 7 (3 Gaussians, symmetric profile), 9 (3 Gaussians, asymmetric profile), 11 (3 Gaussians forming symmetric profile, with 2 additional concentric Gaussians), and 12 (3 Gaussians forming symmetric profile, with hard spheres or Gaussian chains coronas attached). However, it should be emphasized that part of the parameters were in practice only free to vary within relatively narrow intervals due to the structural constraints to these parameters imposed by the model. Details on the different form factors are given in the Appendix.

3. Results

Table 1. Parameter values of the decorated bilayer as obtained from the optimized isotropic SV SAXS model fits shown in Fig. 1. The models consist of concentric Gaussian distributed scattering densities. Parameter values of the corresponding optimized bimodal polydispersity distributions of the SVs are given in the text.

Model	$\rho^*_{c\ in}$ $t_{c\ in}\sqrt{2\pi}$	ρ^*_{in} $t_{in}\sqrt{2\pi}$	ρ^*_{tail} $t_{tail}\sqrt{2\pi}$	ρ^*_{out} $t_{out}\sqrt{2\pi}$	$\rho^*_{c\ out}$ $t_{c\ out}\sqrt{2\pi}$
`3 Gaussians`	–	2.24 a.u.	−1 a.u.	0.05 a.u.	–
`(asymmetric)`	–	1.14 nm	0.97 nm	8.88 nm	–
`3 Gaussians`	–	2.29 a.u.	−1 a.u.	2.29 a.u.	–
`(symmetric)`	–	1.64 nm	2.38 nm	1.64 nm	–
`5 Gaussians`	0.06 a.u.	1.43 a.u.	−1 a.u.	1.43 a.u.	0.40 a.u.
	2.10 nm	1.61 nm	2.11 nm	1.61 nm	1.52 nm

* Normalized to $\rho_{tail} = -1$.

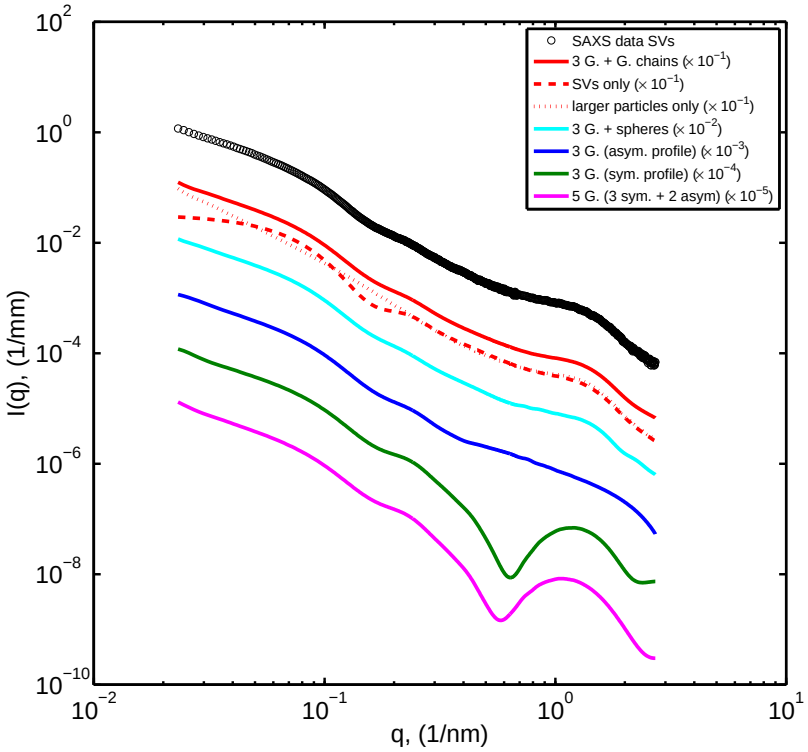

Figure 1. SV SAXS data (○ , black). Fit of anisotropic model (three Gaussians forming symmetric bilayer profile, with Gaussian chains attached) to the SV data (——, red), and contributions to the model calculation originating from the SVs (- - - -, red) and the larger membranous particles (· · · · · ·, red). Corresponding electron density profile and size distribution are given in Fig. 2. Fit of anisotropic model (three Gaussians forming symmetric bilayer profile, with hard spheres attached) to the SV data (——, cyan). Fit of isotropic model (three Gaussians forming asymmetric bilayer profile) to the SV data (——, blue). Fit of isotropic model (three Gaussians forming symmetric bilayer profile) to the SV data (——, dark green). Fit of isotropic model (three Gaussians forming symmetric bilayer profile, plus one additional Gaussian attached to each sides of the profile) to the SV data (——, magenta). Curves partly shifted downwards for clarity, as detailed in the key.

Figure 1 shows data $I(q)$ vs q from SVs in aqueous buffer (○ , black), and least-square fits of isotropic and anisotropic form factor models to the data. The isotropic form factors consist of concentric Gaussians forming symmetric or asymmetric scattering density profiles. Three Gaussians forming a symmetric profile (solid dark green line , *reduced* $\chi^2 = 602$), five Gaussians of which three are forming a symmetric core profile (solid magenta line, *reduced* $\chi^2 = 578$), three Gaussians forming an asymmetric profile (solid blue line, *reduced* $\chi^2 = 34.1$). A bimodal size polydispersity distribution function $p(R)$ was used, with one branch corresponding to cryo-EM data on the size distribution of the SVs, and a second branch corresponding to larger membranous particles, modeled by a freely varied Gaussian distribution.

In addition to the parameters given in Tab. 1 the following parameters have been obtained from the fits (model with three Gaussians (symmetric profile), model with five Gaussians,

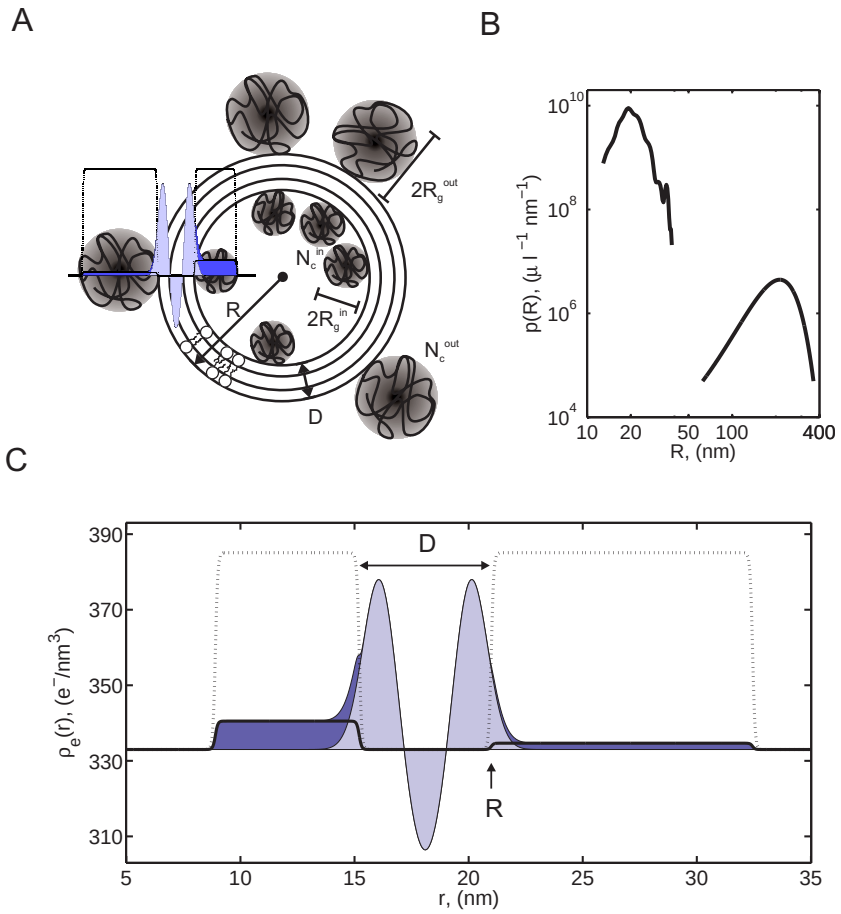

Figure 2. *(A)* Sketch of a real space model corresponding to an optimized scattering form factor consistent with the measured SAXS data from SVs shown in Fig. 1. For details on the model parameters see Table 2, model Gaussian chains coronas, and [3]. *(B)* Bimodal size distribution function $p(R)$ employed in the form factor calculation. Binning size 1 nm. *(C)* Electron density profile $\rho_e(r)$ across a SV membrane corresponding to least-square fit given in Fig. 1 (——red). Typical maximum local contribution of Gaussian chains (· · · · · ·, black), and spherically averaged contribution of Gaussian chains (——, black) are shown. Light blue area: lipid bilayer. Darker blue area: spherically averaged contribution of protein layers. Both $\rho_e(r)$ and $p(R)$ have been calibrated to absolute scales. Adapted from [3].

model with three Gaussians (asymmetric profile)): mean radius larger particles ($\mu = 160.7$ nm, $\mu = 180.1$ nm, $\mu = 127.0$ nm), width distribution larger particles ($\sigma = 45.2$ nm, $\sigma = 50.2$ nm, $\sigma = 51.7$ nm), number larger particles (1.55 %, 1.61 %, 2.47 %) and a small constant background (7×10^{-5} mm^{-1}, 3×10^{-5} mm^{-1}, -3×10^{-5} mm^{-1}). The excess scattering densities ρ_i (relative to aqueous buffer) have been scaled to arbitrary units such that $\rho_{tail} = -1$. Parameters are explicitly defined in the Appendix.

Only the form factor consisting of three Gaussians forming an asymmetric profile is capable to describe the SV SAXS data, at least qualitatively. However, the parameter values of the profile do not correspond to a physically meaningful model. The maximum excess scattering density of the inner leaflet is about 45 times higher than for the outer leaflet. The model parameters would suggest the structure of a lipid monolayer with a thickness of about 3 nm. However, EM

Table 2. Parameter values of the decorated bilayer as obtained from the optimized anisotropic SV SAXS model fits shown in Fig. 1. The models consist of three concentric Gaussians (symmetric bilayer profile), with coronas attached to both sides. Parameter values of the corresponding optimized bimodal polydispersity distributions of the SVs are given in the text.

Model	$\rho^*_{in,out}$ ρ^*_{tail}	$t_{in,out}\sqrt{2\pi}$ $t_{tail}\sqrt{2\pi}$	ρ^*_c	R_g^{in} R_g^{out}	$N_c^{in}/(4\pi(R-D-R_g^{in})^2)$ $N_c^{out}/(4\pi(R+R_g^{out})^2)$
`Hard spheres coronas`[#]	0.18 a.u. -1 a.u.	2.9 nm 0.6 nm	0.28 a.u.	2.4 nm 5.6 nm	13.75×10^{-3} nm^{-2} 0.42×10^{-3} nm^{-2}
`Gaussian chains coronas`	1.63 a.u. -1 a.u.	1.8 nm 2.1 nm	1.81 a.u.	3.2 nm 5.7 nm	7.09×10^{-3} nm^{-2} 0.47×10^{-3} nm^{-2}

[*] Normalized to $\rho_{tail} = -1$.
[#] $R_g^i = R^i$, $i = in,\ out$.

shows a more or less roughly symmetrical bilayer structure of about 5 nm thickness. Further, the indirect Fourier transformation method [17] applied to the SAXS data, followed by the numerical deconvolution of the pair distance distribution function [18, 19, 20] supports the view that a spherical symmetric model is not suited to describe the data (data not shown). Elliptically deformed models consisting of a bilayer profile, similar to the isotropic models above, have been also falsified (data not shown).

The anisotropic models consist of a symmetric core profile (three concentric Gaussians) with either attached hard spheres (solid cyan line, *reduced* $\chi^2 = 4.18$), or with attached Gaussian chains (solid red line, *reduced* $\chi^2 = 2.84$) on both sides of the bilayer profile. The dashed and dotted red lines depict the contributions of the two branches of the bimodal size distribution function $p(R)$ of the model consisting of three Gaussians with Gaussian chains coronas. Again a bimodal size polydispersity distribution function $p(R)$ was used, as defined above.

In addition to the parameters given in Tab. 2 the following parameters have been obtained from the fits (model hard spheres coronas, model Gaussian chains coronas): mean radius larger particles ($\mu = 232.5$ nm, $\mu = 210.1$ nm), width distribution larger particles ($\sigma = 54.5$ nm, $\sigma = 50.2$ nm), number density of larger particles (0.68 %, 0.86 %) and a small constant background. Details on the form factors are given in the Appendix.

Figure 2 (*A*) shows a sketch of a real space model corresponding to the least-squares fit of the form factor consisting of three Gaussians (symmetric profile) with Gaussian chain coronas shown in Fig. 1 (red lines). Figure 2 (*B*) shows the corresponding size distribution function $p(R)$, and (*C*) the electron density profile $\rho_e(r)$ deduced from the optimized model calculation.

Fig. 3 shows data $I(q)$ vs q from a control sample consisting of DOPS vesicles, 20 mg/ml in water (○ , blue), and how they compare to SV data (○ , black). While the data looks qualitatively similar towards both lower and higher q values for the measured interval, the scattered intensities differ up to approximately two orders of magnitude at intermediate q-values. A least-square fit of an isotropic model (three Gaussians, symmetric bilayer profile, and mono-modal Gaussian distributed polydispersity of the particles) to the DOPS data (- - - -, cyan) describes the data well (*reduced* $\chi^2 = 1.07$), although the slight lift-off of the minima towards larger q values of the measured interval, which is usually due to asymmetry of the bilayer profile, is naturally not reproduced by the model calculation employed here [21]. The fit yields for the most frequent radius $\mu = 48.5$ nm, and for the width of the polydispersity distribution $\sigma = 10.2$ nm. The same type of isotropic model (but with a bimodal polydispersity

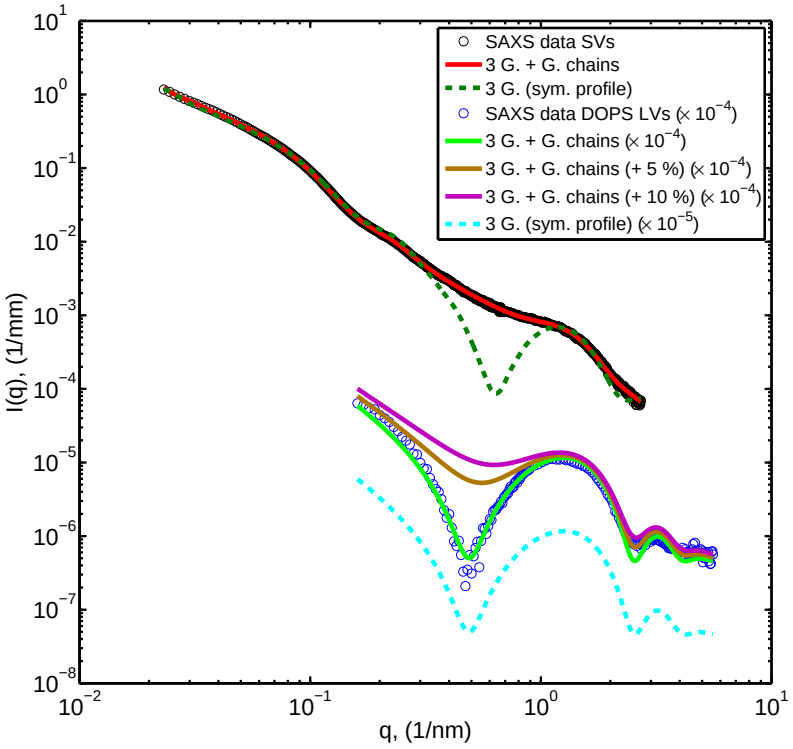

Figure 3. DOPS vesicle data (○ , blue). Fit of isotropic model (three Gaussians, symmetric bilayer profile) to the DOPS data (- - - -, cyan) and anisotropic model with Gaussian chains (——, light green). Anisotropic model with Gaussian chain contributions form SV model added (5 %, ——, brown) and (10 %, ——purple). Curves partly shifted downwards for clarity, as detailed in the key. SVs (○ , black), data identical to data shown in Fig. 1. Fit of isotropic model to the SV data (- - - -, dark green) and anisotropic model with Gaussian chains (——, red).

function) applied to the SV data (- - - -, dark green) fails qualitatively to describe the data, especially in a region around $q \simeq 0.5$ nm^{-1} where data and best-fit deviate by more than one order of magnitude. The fit reveals for the mean of the Gaussian component of the bimodal polydispersity distribution $\mu = 160.7$ nm, for the width $\sigma = 45.2$ nm, and for the number of large particles is 1.54 %.

Least-squares fits of an anisotropic model, similar to the one above but with additional Gaussian chains attached to both sides of the bilayer, to the DOPS data (——, light green) yields almost identical results as the isotropic model (*reduced* $\chi^2 = 1.07$). The size distribution of the liposomes is again assumed to be Gaussian; the fit yields for the polydispersity distribution the most frequent radius $\mu = 48.5$ nm, and a width of $\sigma = 10.2$ nm. In addition, a small constant background was fitted. Interestingly, the number of Gaussian chains in the anisotropic model is zero for the best fit to the DOPS data (within the numerical precision). The qualitative effects of the attached Gaussian chains of the anisotropic model fit to the DOPS data is illustrated by adding 5 % (——, brown) and 10 % (——, purple) of the number of attached Gaussian chains as compared to the corresponding optimized SV model. The parameter values for R_g^{in} and R_g^{out} of the Gaussian chains are taken from the optimized SV model, while the parameter value for

Table 3. Parameter values of the decorated bilayer as obtained from the optimized isotropic and anisotropic SAXS model fits shown in Fig. 3. Parameter values of the corresponding optimized polydispersity distributions of the SVs and DOPS LVs are given in the text.

Sample	Model	$\rho^*_{in,out}$ ρ^*_{tail}	$t_{in,out}\sqrt{2\pi}$ $t_{tail}\sqrt{2\pi}$	ρ^*_c	R_g^{in} R_g^{out}	$N_c^{in}/(4\pi(R-D-R_g^{in})^2)$ $N_c^{out}/(4\pi(R+R_g^{out})^2)$
SVs	isotropic[#]	2.29 a.u. −1 a.u.	1.64 nm 2.38 nm	–	– –	– –
SVs	anisotropic[$]	1.63 a.u. −1 a.u.	1.8 nm 2.1 nm	1.81 a.u.	3.2 nm 5.7 nm	7.09×10^{-3} nm^{-2} 0.47×10^{-3} nm^{-2}
DOPS LVs	isotropic	2.24 a.u. −1 a.u.	0.89 nm 2.81 nm	–	– –	– –
DOPS LVs	anisotropic	2.24 a.u. −1 a.u.	0.89 nm 2.81 nm	1.30 a.u.	3.9 nm 4.0 nm	$< 1\times10^{-13}$ nm^{-2} $< 1\times10^{-13}$ nm^{-2}
DOPS LVs	anisotropic (+ 5 % G. chains)	2.24 a.u. −1 a.u.	0.89 nm 2.81 nm	2.49 a.u.	3.2 nm 5.7 nm	3.55×10^{-3} nm^{-3} 0.24×10^{-3} nm^{-3}
DOPS LVs	anisotropic (+ 10 % G. chains)	2.24 a.u. −1 a.u.	0.89 nm 2.81 nm	2.49 a.u.	3.2 nm 5.7 nm	7.09×10^{-3} nm^{-3} 0.47×10^{-3} nm^{-3}

[*] Normalized to $\rho_{tail} = -1$.
[#] Identical to model fit "3 Gaussians (symmetric)" in Table 1.
[$] Identical to model fit "Gaussian chains coronas" in Table 2.

Table 4. Parameter values as obtained from the optimized anisotropic SAXS model fits shown in Fig. 4

Model fit parameter	Native SVs	SVs protease	Unit
ρ_{in}, ρ_{out}	1.58	1.50	a.u.
ρ_{tail}	−1	−1	a.u.
$t_{in}\sqrt{2\pi}$, $t_{out}\sqrt{2\pi}$	1.9	1.7	nm
$t_{tail}\sqrt{2\pi}$	2.1	2.4	nm
R_g^{in}	2.8	2.6	nm
R_g^{out}	5.7	5.9	nm
$N_c^{in}/(4\pi(R-D-R_g^{in})^2)$	15.04×10^{-3}	8.73×10^{-3}	nm^{-2}
$N_c^{out}/(4\pi(R+R_g^{out})^2)$	0.27×10^{-3}	0.15×10^{-3}	nm^{-2}
ρ_c	1.84	1.73	a.u.
μ	210.5	211.0	nm
σ	49.7	51.1	nm
Number larger particles	0.86	0.68	%
Constant background	3.67×10^{-4}	15.5×10^{-4}	mm^{-1}

ρ_c is calculated relative to $\rho_{in} = \rho_{out}$ to have the same value as for the optimized SV model. A least-squares fit of the anisotropic model to the SV data (——, red, same fit as in Fig. 1) is in excellent agreement with the data, while employing physiological and biochemical meaningful parameter values [3, 2].

Fig. 4 shows the SAXS intensity function $I(q)$ vs. q for a SV sample (black circles) and SV treated with a Trypsin protease (blue circles) and corresponding least-squares fits (*reduced* $\chi^2 = 0.66$, and *reduced* $\chi^2 = 0.51$, respectively) to the form factor model (solid red

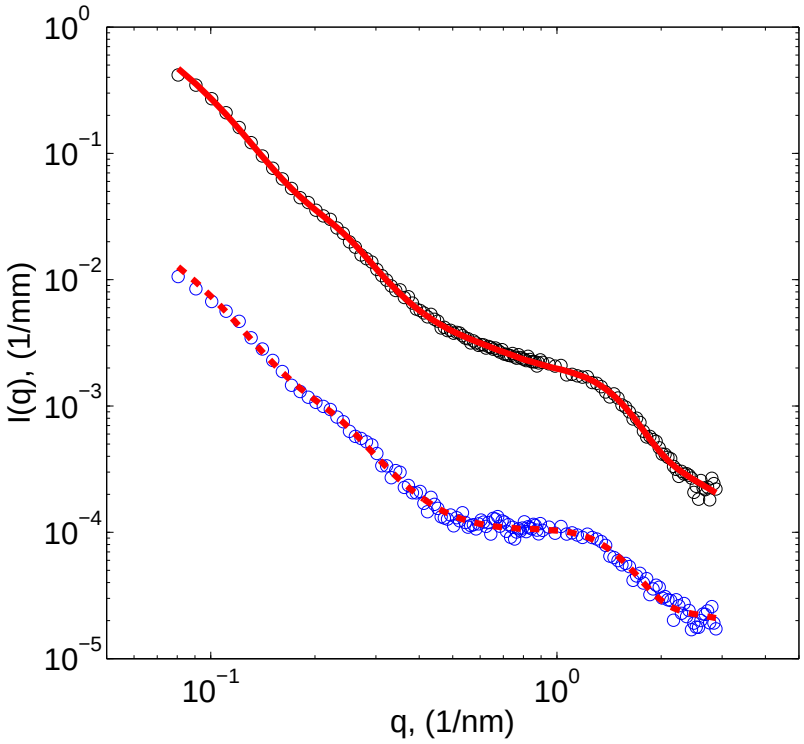

Figure 4. SVs with additional centrifugation in purification protocol (○ black), and SVs treated with protease to remove protein residues facing outwards, also with an additional centrifugation in purification protocol (○ blue, shifted by factor 0.1 for clarity). Fit of anisotropic model with Gaussian chains attached to the SV data (——red, and - - - -red, shifted by factor 0.1 for clarity).

line, and dashed red line, respectively) for bilayer vesicles with Gaussian chains attached to the inside and outside, as detailed in the Appendix. Again a bimodal size polydispersity distribution function $p(R)$ was used, with the left branch corresponding to the cryo-EM data of SVs centered around 21 nm, and the right branch corresponding to the larger membranous particles, modeled by a Gaussian distribution centered around $\mu \approx 210$ nm with a standard deviation of $\sigma \approx 50$ nm. It should be emphasized that due to the resolution of the SAXS technique, our data are relatively insensitive to the exact size distribution of these larger particles. The errors appear to slightly overestimate the actual variances, as the model fit does not over fit the data, even though we obtain $\chi^2 < 1$ for both fits. The parameters of the fits are given in Tab. 4. Most parameter values do not change much when comparing the results from the fit to the SVs (with additional centrifugation step in the purification protocol) data and the protease treated SV sample, also with additional centrifugation step. But, importantly, the number density of Gaussian chains facing the lumen and the outside are both reduced by about a factor of two as an effect of the protease treatment of the sample.

4. Discussion

In combination with complimentary techniques such as cryo-EM and biochemical analysis, we have shown that SAXS is capable of elucidating structures of significant complexity such as SVs.

State of the art beamlines have been used to record the SAXS data, which were found to

be highly reproducible [3]. As we show in Fig. 1, several different isotropic models have been discussed and have been falsified. After assessment of numerous samples, we are convinced that the presented effective model representing proteins in a coarse-grained sense by Gaussian chains is well suited to describe the SVs quantitatively at the given resolution.

However, possible ambiguities and model dependencies of the results are important issues, which need to be addressed explicitly. We have therefore compared fits with two independent anisotropic models that share the main features of anisotropic protein clusters, but use different detailed implementations. In particular, the clustered proteins are represented by hard spheres in the first, and by Gaussian chains in the second. Importantly, these two models show qualitatively similar results, and thus support the main conclusion that an anisotropic model is needed to accurately describe the SV data. Of course, to some extent the derived model parameters of the observed clustering effect are different. These differences mark the degree to which the results depend on the specific formulation of the model, see Tab. 2. The main conclusions and existence of protein clusters are, however, maintained in a model independent way.

Models where the proteins are represented by spherically symmetric Gaussian electron densities as depicted in Fig. 3 illustrate the effects that the Gaussian chains parameters, or hard spheres parameters, have on the scattering curve. In an intermediate q-range, the difference in scattering length of the SV data, when compared to unilamellar DOPS vesicles is found to be in excess of two orders of magnitude.

Importantly, least squares model fits to the DOPS data yield almost identical results for a spherically symmetric model with a symmetric density profile of three coupled Gaussians (Fig. 3, dashed cyan line), and a model with Gaussian chains attached to the profile (Fig. 3, solid light green line). Interestingly, the number of Gaussian chains in the later model is zero for the best fit (within the numerical precision). Models with significant amounts of attached Gaussian chains with parameter values similar to the ones from the corresponding optimized SV model can be falsified against the DOPS data Fig. 3, solid brown line, and solid purple line).

The mathematical model utilized to fit the experimental data contains 12 parameters to account for the structural complexity of the SV sample. Given the high complexity of the system, the high number of data points (up to 763) and the wide q-range of the data, a model form factor fit with 12 parameters is perfectly justified. We have verified that the model components are both necessary and sufficient to accurately describe the data, see also the reduced, and alternative model fits in Fig. 1 and Fig. 3. None of the contributions are marginal, neither within the model structure of one particle, nor considering the two branches of the polydispersity distribution $p(R)$.

In addition, the values for several parameters can be constrained fairly well due to information from cryo-EM and additional biochemical knowledge. The fact that SVs are known to have a unilamellar bilayer structure with incorporated and attached proteins introduces several constrains to the model parameters. Further, the size distribution of the larger particles can be estimated, at this point only qualitatively, by cryo-EM. The investigated q-range is not very sensitive to the precise size of particles in the size range of the larger particles. Due to the heterogeneous nature and broad size distribution of these particles, pronounced features at lower q regions cannot be expected. Particular features outside the measurement interval do not appear in the model calculations, either at small or at high q, i.e. the measurement range (after stitching different detector distances) was well adapted. In particular, the heterogeneous nature and broad size distribution of the larger particles suppressed any pronounced features at lower q-ranges.

Let us now consider the relative contributions to the measured SV SAXS curves, of photons scattered from particles belonging to the two branches of the polydispersity function $p(R)$, namely SVs and larger membranous particles, which can be considered as a contamination. Importantly, the relative scattering contributions of particles, and parts of particles, of different

sizes depend strongly on the considered value of q.

The number density of the actual SVs is about 100 times higher as the number density of the larger particles. The factor of about 10 in size difference of the particles gives a factor of about 100 in favor of the larger structures considering the relative surface areas of the particles. This is because the part of the reciprocal space studied here contains mainly information about length scales in the order of the thickness of the protein covered bilayer. This leads to approximately equal numbers of photons scattered into the measured q-range from particles belonging to either branch of $p(R)$. Comparing this result to the relative number of photons scattered into the entire reciprocal space (q-integrated) from the two branches of $p(R)$ this means that about 99 % of the scattering intensity due to the larger particles is expected to be scattered into lower q-regions, as compared to the q-interval measured here. The results of these considerations correspond well with the contributions from the two branches of $p(R)$ in the model fit calculation shown in Fig. 1, (red lines).

SVs which are treated with Trypsin from the outside show distinct scattering curves when compared to data from native SVs (open black, and blue circles, in Fig. 4). Least-squares fits to a form factor model (symmetric bilayer profile with attached Gaussian chains) result in a reduction of scattering mass attributed to the Gaussian chains, both inside and outside. This may be due to the fact that the attached Gaussian chains facing the lumen and the outside of the SV model account to some extent in a similar manner for structures on the SV sticking both towards the inside and the outside. Alternatively, the protease treatment may also cause disintegration of the protein clusters on the SVs, thus affecting the organization of proteins facing outwards and inwards. Further, although it seems highly unlikely, it can not be ruled out completely at this point that the protease might have penetrated into the SVs, and subsequently removed protein residues from both sides of the SV membrane. Electron micrographs of the protease treated SVs show no evidence of penetration of the protease into the SVs (data not shown). However, EM is not capable of strictly excluding such a scenario. In other experiments, we have used protease treatment of SVs many times (using harsher conditions than those shown here) followed by checking the intravesicular fragments of synaptotagmin, synaptophysin, and synaptogyrin. For all these proteins, fragments of the expected molecular mass were detectable (that are degraded when the membranes are solubilized), showing that there is efficient protection of the vesicle interior. Importantly, breaking of spherical symmetry still remains an essential ingredient in order to obtain a good fit.

The results from the fit of the SVs with an additional centrifugation step in the purification protocol as compared to the results obtained from SV samples following the usual purification protocol, see Tab. 3 and [3] show different number densities of the Gaussian chains attached to both sides of the bilayer profile. The number density of Gaussian chains facing the inside of the SVs $N_c^{in}/(4\pi(R-D-R_g^{in})^2)$ is increased by about a factor of two, while the number density of Gaussian chains facing the outside $N_c^{out}/(4\pi(R+R_g^{out})^2)$ is decreased by about a factor of two. At the moment the significance and possible reasons of this discrepancy remains unclear, since the usual SV purification protocol already contains several centrifugation steps similar to the additional one needed to remove the Trypsin and the protein fragments from the protease treated SVs.

5. Summary and perspective

In summary, we have discussed different spherically symmetric and anisotropic form factor models and have tested them against high resolution SAXS data from SVs, isolated from rat brain. Anisotropy of the model form factors is found to be a key ingredient for the description of the native SV structure. After protease digestion of the surface of the SVs (unspecific protein removal), a significant reduction of the anisotropic terms is observed. This compares well with the observation, that the anisotropic terms in the form factor vanish in least-squares fits of

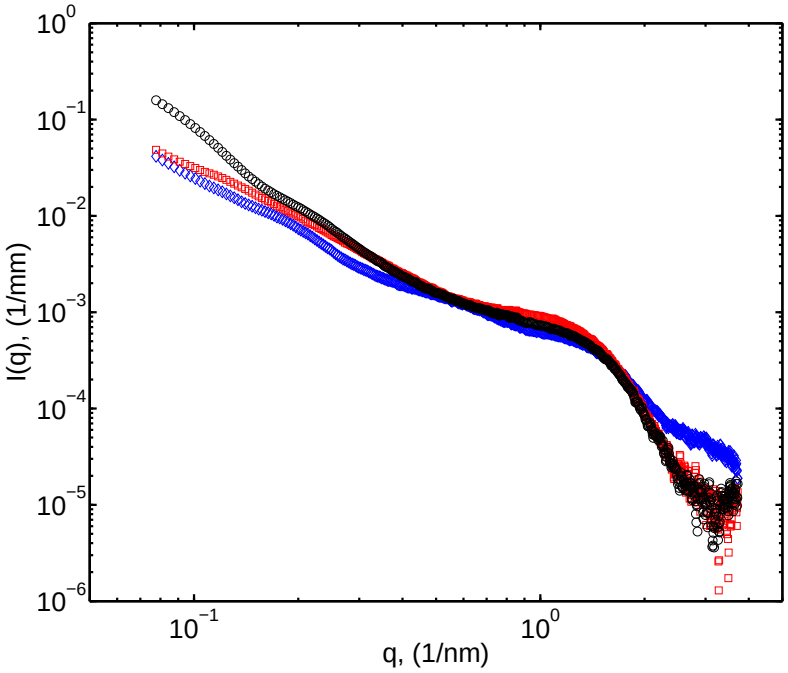

Figure 5. SVs at pH 7.40 (○ black), SVs at low (2.1) pH (◇blue), and SVs at high (12.9) pH (□red).

SAXS data from small unilamellar vesicles composed of DOPS. These vesicles are spherically symmetric on the experimentally resolved length scales. Besides the excellent agreement with the SAXS data, the suggested SV form factor model is consistent with published electron microscopy, biochemical and physiological data. Furthermore, we have presented SAXS data of SVs recorded under different pH conditions, and have described changes in structural parameters due to protease digestion of SVs.

In terms of further structural analysis of SVs, changes in structure as a function of physiological conditions (pH, ion concentration, osmotic pressure etc.) are obvious candidates for investigation.

As a first example, Fig. 5 shows data from SV samples in HB100 buffer at pH 2.1, pH 7.4 and pH 12.9. The SAXS curves show distinct features depending on the pH conditions. The overall slope of the scattering curves is decreased at both high and low pH conditions as compared to neutral pH. This might be due to changes in overall shape and/or size of the SVs. Also aggregation (docking) of SVs might lead to this effects. Resolved changes in the higher q-regions of the recorded data indicate distinct changes in the local structure of the protein decorated bilayer of the SVs as a function of pH conditions. The underlying detailed structural changes are to be further investigated and remain unclear at present. However, the SVs seem to retain well defined structures even under extreme pH conditions. More subtle changes of the chemical environment of the SV samples like different calcium concentrations in the range of 0 to 100 μM, or magnesium concentrations around 200 mM did not show resolvable differences in the corresponding SAXS curves (data not shown).

A particular advantage of the method is the lack of invasive sample preparation steps, such as the fixation and staining needed for electron microscopy, which can introduce artifacts into the analysis. Owing to the small sample quantities needed for high brilliance synchrotron SAXS

(on the order of 10^{-4} to 10^{-3} μl), a large number of samples can be collected and compared in a batch. Comparable sample series would consume too much time and material using other techniques (in-house SAXS, transmission electron microscopy etc.). Our present SAXS data has employed scattering intensities up to $q = 2.7$ nm^{-1}. By increasing the final vesicle concentration, through modifications in the purification protocol, this range could be extended. For example, with a theoretical concentration increase of 100-fold, the exploitable q-range should be extended by a factor of three, reaching a resolution of about 0.8 nm. Structural studies of vesicles isolated from wild-type animals could also be augmented by using so-called "knock-in" and "knock-out" animals, to genetically manipulate essential components of the system (Holt and Jahn, manuscript in preparation). Furthermore, SAXS could be employed to determine time-resolved structural changes resulting from membrane fusion, in combination with microfluidic devices.

With the advent of x-ray lasers delivering ultra short and extremely intensive x-ray pulses, time resolved scattering experiments at individual organelles and fusion intermediates might eventually become possible. Such experiments would undoubtedly shed light on the biophysical principles of membrane merger.

Acknowledgments
The authors thank Maria Druminski for help with the SV preparations and Dietmar Riedel for EM measurements. SC thanks Otto Glatter for enlightening discussions regarding inversion of scattering data. This work was financially supported by the "Excellence Cluster Initiative 171/Deutsche Forschungsgemeinschaft (DFG) Research Center 103 – Center for Molecular Physiology of the Brain", as well as DFG SFB 803 and the Max Planck Society. European Synchrotron Radiation Facility and Hamburger Synchrotronstrahlungslabor at Deutsches Elektronen-Synchrotron are acknowledged for beamtime and excellent working conditions.

Appendix A. Scattering Form Factor Models

Appendix A.1. Isotropic Form Factor Models

Equation A.2 (below) gives the final form factor of the isotropic models used in the fitting procedures. The models are built from a central symmetric or asymmetric bilayer profile, with added spherically symmetric protein shells on the inside (lumen) and outside of the SV. The bilayer electron density profile is modeled by three concentric Gaussians [11], representing the headgroups of the two lipid leaflets and the hydrophobic core. Note amino acid residues associated with the headgroups and trans-membrane protein segments are included in this contribution. The inner and outer protein shells are modeled by concentric Gaussians attached to the inner and outer sides of the bilayer, respectively. The excess scattering length density of the bilayer profile is given by

$$\rho(r) = \sum_i \rho_i \exp\left(-\frac{(r-R_i)^2}{2t_i^2}\right), \tag{A.1}$$

with the peak position R_i, amplitude ρ_i and width t_i with $i \in$ *in*, *out*, *tail*, *inner*, *outer*, for each of the three Gaussians representing the headgroups of the two leaflets and the tail region, and the inner and outer protein shell, respectively. The (characteristic) radius R is defined as $R = R_{out} + t_{out}\sqrt{2\pi}/2$ mimicking a SV with the outer lipid bilayer surface at $r \simeq R$. To reduce the number of model parameters, we choose $R_{tail} = R - (t_{out} + t_{tail}/2)\sqrt{2\pi}$, $R_{in} = R - (t_{out} + t_{tail} + t_{in}/2)\sqrt{2\pi}$. Thus, the total thickness D of the bilayer is characterized by $D = \sqrt{2\pi}(t_{in} + t_{tail} + t_{out})$. Further, we choose $R_{inner} = R - (t_{out} + t_{tail} + t_{in} + t_{inner}/2)\sqrt{2\pi}$ and $R_{outer} = R + (t_{outer}/2)\sqrt{2\pi}$ so that the overall thickness of the synaptic membrane is characterized by the total thickness D of the bilayer structure and the thickness of the inner and outer protein layers. The total excess scattering length with respect to the aqueous buffer is

β_b. Depending on the specific model, we choose (1) $t_{in} = t_{out}$ (symmetric bilayer), (2) $t_{in} \neq t_{out}$ (asymmetric bilayer), or (3) $\rho_{inner} = \rho_{outer} = 0$ (no protein shells). Note that the Gaussians representing the bilayer profile and the protein shells interpenetrate to some extent due to their tails.

The form factor corresponding to the above model can be calculated in kinematic scattering theory, yielding the following result

$$P(q,R) = \frac{1}{M^2}\beta_b^2 F_b^2(q,R) \ . \tag{A.2}$$

The symbols and functions are given below: $M = \beta_b$ denotes the excess scattering length. The normalized amplitude of the self-correlation term of the bilayer profile and the isotropic protein shells is given by

$$F_b(q,R) = \frac{1}{\beta_b}\sum_i \beta_{b\ i} F_{b\ i}(q,R_i) \ , \tag{A.3}$$

with $i \in$ *in*, *out*, *tail*, *inner*, *outer*, and

$$F_{b\ i}(q,R_i) = \frac{1}{\beta_{b\ i}} 4\sqrt{2}\pi^{3/2} t_i \rho_i \exp\left(-\frac{t_i^2 q^2}{2}\right)\frac{1}{q}[t_i^2 q\cos(qR_i) + R_i \sin(qR_i)] \ , \tag{A.4}$$

where $\beta_{b\ i} = \rho_i \frac{4\pi}{3}((R_i + t_i\sqrt{2\pi}/2)^3 - (R_i - t_i\sqrt{2\pi}/2)^3)$ denotes the excess scattering mass of one peak of the profile [11].

Appendix A.2. Anisotropic Form Factor Models

Equation A.5 (below) gives the final form factor for the anisotropic model with Gaussian chains coronas used in the fitting procedure. The model is built from a central bilayer profile with added protein coronas on the inside (lumen) and outside of the SV model.

The bilayer electron density profile is modeled by three concentric Gaussians [11], representing the headgroups of the two lipid leaflets and the hydrophobic core. Note amino acid residues associated with the headgroups and trans-membrane protein segments are included in this contribution. The inner and outer protein shells are modeled by Gaussian chains [12] attached to the inner and outer sides of the bilayer, respectively [13, 14, 15, 16]. The excess scattering length density of the bilayer profile is given by Eq. A.1 with $i \in in, out, tail$, for each of the three Gaussians representing the headgroups of the two leaflets and the tail region, respectively. The (characteristic) radius R, R_{tail}, R_{in}, D and β_b are defined as for the the isotropic form factor models. To reduce the number of model parameters further, we choose $t_{in} = t_{out}$ (symmetric bilayer). There are N_c^{in} and N_c^{out} Gaussian chains distributed randomly and without correlations forming the inner and outer protein shell, respectively. The individual Gaussian chains are characterized by their root-mean-square radius of gyration, R_g^{in} and R_g^{out}, and their common average excess scattering length density ρ_c. The distance between the inner headgroup maximum of the bilayer profile and the center of mass of the Gaussian chains facing the lumen is taken to be $t_{in}\sqrt{2\pi}/2 + R_g^{in}$, and the distance between the outer headgroup maximum and the center of mass of the Gaussian chains facing outwards is taken to be $t_{out}\sqrt{2\pi}/2 + R_g^{out}$. This limits the penetration of the Gaussian chains into the bilayer, although there is some remaining overlap, mostly due to the extending tails of the bilayer profile [13]. The form factor corresponding to

the above model can be calculated in kinematic scattering theory, yielding the following result

$$\begin{aligned} P(q,R) = \frac{1}{M^2} \times [\quad & \beta_b^2 F_b^2(q,R) \\ & + \sum_{i=in,out} N_c^i \beta_c^{i\ 2} P_c^i(q) \\ & + \sum_{i=in,out} 2N_c^{i\ 2} \beta_b \beta_c^i S_{b\ c}^i(q,R) \\ & + \sum_{i=in,out} N_c^i (N_c^i - 1) \beta_c^{i\ 2} S_c^i(q,R) \\ & + S_c^{in\ out}(q,R) \prod_{i=in,out} N_c^i \beta_c^i \ ] \ . \end{aligned} \tag{A.5}$$

The symbols and functions are given below: $M = \beta_b + N_c^{in}\beta_c^{in} + N_c^{out}\beta_c^{out}$ denotes the excess scattering length, with $\beta_c^i = \rho_c {R_g^i}^3 4\pi/3$ and $i = in, out$ representing the total excess scattering length of a single chain on the outside and on the inside of the bilayer profile, respectively. The normalized amplitude of the self-correlation term of the bilayer profile is given by Eq. A.3 with Eq. A.4 where $\beta_{b\ i}$ is defined as for the isotropic form factor models.

The self-correlation terms of the Gaussian chains are given by Debye functions

$$P_c^i(q) = \frac{2[\exp(-x^i) - 1 + x^i]}{x^{i\ 2}} \ , \tag{A.6}$$

with $x^i = q^2 R_g^{i\ 2}$ and $i = in, out$ for the inner and outer chains, respectively. The interference cross-terms $S_{b\ c}^{in}(q,R)$ and $S_{b\ c}^{out}(q,R)$ between the bilayer and the Gaussian chains on the inside and outside, are given by

$$S_{b\ c}^i(q,R) = F_b(q,R)\psi^i(x^i)\frac{\sin(q[R_{tail} \mp (D/2 + R_g^i)])}{q[R_{tail} \mp (D/2 + R_g^i)]} \ , \tag{A.7}$$

with $i = in, out$ and $\psi^i(x^i) = [1 - \exp(-x^i)]/x^i$ the effective form factor amplitude of the Gaussian chains [22]. The product of the scattering form factor amplitudes of the chains belonging to one of the chain layers with the scattering form factor amplitude of a infinite thin shell is equivalent to a convolution of the corresponding scattering density distributions in real space [14] and accounts for the fact that the Gaussian shells are located on a spherical shell.

$$S_c^i(q,R) = \left(\psi^i(x^i)\frac{\sin(q[R_{tail} \mp (D/2 + R_g^i)])}{q[R_{tail} \mp (D/2 + R_g^i)]} \right)^2 \ , \tag{A.8}$$

with $i = in, out$. The interference term between the chains of the inner and outer shells is taken into account by

$$S_c^{in\ out}(q,R) = \prod_{i=in,out} \psi^i(x^i)\frac{\sin(q[R_{tail} \mp (D/2 + R_g^i)])}{q[R_{tail} \mp (D/2 + R_g^i)]} \ . \tag{A.9}$$

The anisotropic form factor, where spherical particles were placed on the inside and outside of a symmetric bilayer profile instead of the Gaussian chains, is similar to that given in Eq. A.5, except that P_c^i in Eq. A.6 and ψ^i in Eq. A.7 are replaced by the scattering form factor of spheres and the scattering form factor amplitude of spheres, respectively. The spheres are of radii R^{in} and R^{out}, the number of free parameters is the same as for the model with the attached Gaussian chains.

References

[1] Südhof T C 2004 *Annu. Rev. Neurosci.* **27** 509 – 547
[2] Takamori S, Holt M, Stenius K, Lemke E A, Grønborg M, Riedel D, Urlaub H, Schenck S, Brügger B, Ringler P, Müller S A, Rammner B, Gräter F, Hub J S, De Groot B L, Mieskes G, Moriyama Y, Klingauf J, Grubmüller H, Heuser J, Wieland F and Jahn R 2006 *Cell* **127** 831 – 846
[3] Castorph S, Riedel D, Arleth L, Sztucki M, Jahn R, Holt M and Salditt T 2010 *Biophys. J.* **98** 1200–1208
[4] Hell J W, Maycox R P, Stadler H and Jahn R 1988 *EMBO J.,* **7** 3023 – 3029
[5] Narayanan T, Diat O and Boesecke P 2001 *Nucl. Instrum. Methods Phys. Res., Sect. A* **467** 1005 – 1009
[6] Haubold H G, Gruenhagen K, Wagener M, Jungbluth H, Heer H a A, Rongen H, Brandenberg G, Moeller R, Matzerath J, Hiller P and Halling H 1989 *Rev. Sci. Instrum.* **60** 1943 – 1946
[7] Guinier A and Fournet G 1955 *Small Angle Scattering of X-rays* (New York: Wiley Interscience)
[8] Bouwstra J A, Gorris G S, Bras W and Talsma H 1993 *Chemistry and Physics of Lipids* **64** 83 – 98
[9] Pabst G, Rappolt M, Amenitsch H and Laggner P 2000 *Phys. Rev. E* **62** 4000 – 4009
[10] Pabst G, Koschuch R, Pozo-Navas B, Rappolt M, Lohner K and Laggner P 2003 *J. Appl. Cryst.* **36** 1378 – 1388
[11] Gradzielski M, Langevin D, Magid L and Strey R 1995 *J. Phys. Chem.* **99** 13232 – 13238
[12] Debye P 1947 *J. Phys. Colloid Chem.* **51** 18 – 32
[13] Pedersen J S and Gerstenberg M C 1996 *Marcromolecules* **29** 1363 – 1365
[14] Pedersen J S 2000 *J. Appl. Cryst.* **33** 637 – 640
[15] Pedersen J S 2001 *J. Chem. Phys.* **114** 2839 – 2846
[16] Arleth L and Vermehren C *J. Appl. Cryst.* Submitted
[17] Glatter O 1977 *J. Appl. Cryst.* **10** 415–421
[18] Glatter O 1981 *J. Appl. Cryst.* **14** 101–108
[19] Glatter O and Hainisch B 1984 *J. Appl. Cryst.* **17** 435–441
[20] Mittelbach R and Glatter O 1998 *J. Appl. Cryst.* **31** 600–608
[21] Kucerka N, Gallová J, Uhrıková D, Balgavỳ P, Bulacu M, Marrink S and Katsaras J 2009 *Biophys. J.* **97** 1926–1932
[22] Hammouda B 1992 *Journal of Polymer Science B* **30** 1387 – 1390